Lateral Casimir Force on a Rotating Particle near a Planar Surface

Alejandro Manjavacas,[1,*] Francisco J. Rodríguez-Fortuño,[2,†] F. Javier García de Abajo,[3,4] and Anatoly V. Zayats[2]
[1]Department of Physics and Astronomy, University of New Mexico, Albuquerque, New Mexico 87131, USA
[2]Department of Physics, King's College London, London WC2R 2LS, United Kingdom
[3]ICFO—Institut de Ciencies Fotoniques, The Barcelona Institute of Science and Technology, 08860 Castelldefels (Barcelona), Spain
[4]ICREA—Institució Catalana de Recerca i Estudis Avançats (ICREA), Passeig Lluís Companys 23, 08010 Barcelona, Spain
(Received 8 December 2016; published 31 March 2017)

We study the lateral Casimir force experienced by a particle that rotates near a planar surface. The origin of this force lies in the symmetry breaking induced by the particle rotation in the vacuum and thermal fluctuations of its dipole moment, and therefore, in contrast to lateral Casimir forces previously described in the literature for corrugated surfaces, it exists despite the translational invariance of the planar surface. Working within the framework of fluctuational electrodynamics, we derive analytical expressions for the lateral force and analyze its dependence on the geometrical and material properties of the system. In particular, we show that the direction of the force can be controlled by adjusting the particle-surface distance, which may be exploited as a new mechanism to manipulate nanoscale objects.

DOI: 10.1103/PhysRevLett.118.133605

Fluctuation-induced forces exist between polarizable atoms, nonpolar molecules, and structured materials, emerging as a result of vacuum and thermal fluctuations that involve virtual electromagnetic excitations. Specifically known as van der Waals or London dispersion forces at short-range distances, Casimir-Polder forces when taking retardation into account, and Casimir-Lifshitz forces when including material dispersion, these are generally referred to as Casimir forces [1–3]. There is strong evidence that various phenomena in nature such as adhesion, friction, wetting, and stiction are a result of these forces [4], and therefore, their study can shed light onto the mechanical behavior of nanodevices, where these forces may play a dominant role [5,6].

Casimir forces are typically attractive, acting along symmetry directions (e.g., the normal to the interacting surfaces [7,8]). However, if the surfaces are corrugated, these forces may have a component parallel to the surface, which is commonly referred to as *lateral* [9–12]. The lateral Casimir force has been successfully measured and has been argued to enable interesting applications such as contactless transmission of lateral motion [13–17]. Nevertheless, the force still acts along local surface-normal directions and arises due to the broken mirror symmetry introduced by the corrugations. Therefore, it strongly depends on the mutual geometric lateral displacement between the corrugations on both surfaces, becoming zero when they are aligned and the lateral mirror symmetry is recovered. Lateral forces have been also predicted for anisotropic particles near surfaces in the absence of thermal equilibrium [18].

In this Letter, we describe a lateral Casimir force that acts on a rotating particle near an ideally flat surface. This lateral force is directed parallel to the surface. The geometry under consideration (Fig. 1) has translational symmetry in the direction of the force; however, the symmetry is broken by the rotation of the particle, leading to the observed force. Rotating particles have been shown to experience Casimir frictional torques that slow down their motion [19–21]. Here, we analyze a qualitatively different effect: a lateral force that pushes the particle parallel to the surface and has direction and magnitude determined by the sense and frequency of rotation, the particle-surface distance, and the materials from which the particle and the surface are made. The force does not depend on the lateral position of the particle due to the translational invariance of the surface and is consistent with the frictional force predicted to exist between surfaces in relative uniform motion [22].

The system investigated here constitutes a Casimir analogue of a mechanical wheel rotating and moving over a planar surface but with no contact required. The origin of this force can be traced back to the recently discovered spin-direction locking of electromagnetic evanescent waves [23–25], an example of the spin-orbit coupling of light [26]. Lateral optical forces [27–29] naturally arise from an asymmetric scattering by circularly polarized dipoles into

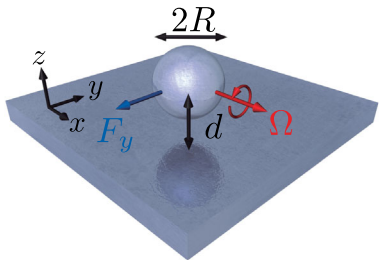

FIG. 1. Sketch of the system under study. A spherical nanoparticle of radius R is rotating with angular frequency Ω at a center-to-surface distance d above a planar surface. Because of the rotation, the particle experiences a lateral force F_y.

electromagnetic modes of any neighboring surface or waveguide [30–32]. Similarly, the rotating particle experiences an imbalance between left- and right-handed helicities in the vacuum and thermal fluctuations associated with its electromagnetic response, which ultimately leads to the lateral Casimir force predicted in this work.

Theoretical model.—We consider a spherical particle small enough to be adequately described within the dipolar limit through a frequency-dependent polarizability $\alpha(\omega)$. The particle rotates around the x axis, parallel to a planar surface located at $z = 0$, with rotation frequency Ω, as shown in Fig. 1. The rotation modifies the interaction of the particle with the vacuum and thermal electromagnetic fields. In particular, in a frame rotating with the particle, an external circularly polarized (CP) electromagnetic field is perceived with a reduced ($\omega_- = \omega - \Omega$) or increased ($\omega_+ = \omega + \Omega$) frequency depending on whether the handedness of the field coincides with ($\hat{\boldsymbol{\sigma}}_+$) or is opposed to ($\hat{\boldsymbol{\sigma}}_-$) the particle rotation, respectively. This results in the splitting of the polarizability of the nonrotating particle into two components $\alpha_+(\omega) = \alpha(\omega_-)$ and $\alpha_-(\omega) = \alpha(\omega_+)$ associated with the unit vectors of opposite CP field helicities $\hat{\boldsymbol{\sigma}}_+ = (1/\sqrt{2})(\hat{\mathbf{y}} + i\hat{\mathbf{z}})$ and $\hat{\boldsymbol{\sigma}}_- = (1/\sqrt{2})(\hat{\mathbf{y}} - i\hat{\mathbf{z}})$. Because the vacuum and thermal fluctuations of the dipole moment of the particle are determined by its effective polarizability through the fluctuation-dissipation theorem (FDT) [19,33–35], the imbalance in the circularly polarized components results in asymmetric fluctuations that are the origin of the lateral force, as discussed above [27–32].

In order to obtain an analytical expression for the lateral Casimir force, we start by considering the electromagnetic force acting on a dipole $\mathbf{p}$ in an electric field $\mathbf{E}$, which can be written as $\mathbf{F} = \sum_i p_i \nabla E_i$ [36], with $i = x, y, z$. The vacuum and thermal fluctuations causing the Casimir force come from two different sources: (i) fluctuations of the dipole moment of the particle $\mathbf{p}^{\mathrm{fl}}$ and (ii) the field $\mathbf{E}^{\mathrm{fl}}$ generated by current fluctuations in the surface. As these two sources of fluctuations originate in different systems, they are uncorrelated, and therefore $F_y = \sum_i \langle p_i^{\mathrm{fl}} \partial_y E_i^{\mathrm{ind}} + p_i^{\mathrm{ind}} \partial_y E_i^{\mathrm{fl}} \rangle$, where $\langle\rangle$ stands for the average over fluctuations, which we perform using the FDT. Now, expressing the induced field in terms of the fluctuating dipole with the help of the surface Green function $\bar{G}$ and the induced dipole in terms of the fluctuating field as $\mathbf{p}^{\mathrm{ind}} = \bar{\alpha}_{\mathrm{eff}} \mathbf{E}^{\mathrm{fl}}$, we obtain (see Supplemental Material [37] for details)

$$F_y = \frac{\hbar}{\pi} \int_0^\infty d\omega \mathrm{Im}\{\partial_y G_{yz}(\omega) - \partial_y G_{zy}(\omega)\} \times [\mathrm{Im}\{\alpha(\omega_+)\} N(\omega_+) - \mathrm{Im}\{\alpha(\omega_-)\} N(\omega_-)], \quad (1)$$

where $N(\omega_\pm) = n(T_1, \omega_\pm) - n(T_0, \omega)$, with $n(T_i, \omega) = [\exp(\hbar\omega/k_B T_i) - 1]^{-1}$ being the Bose-Einstein distribution at temperature T_i, and T_0 and T_1 the temperatures of the surface and the particle, respectively. Interestingly, the lateral Casimir force is finite even for $T_1 = T_0 = 0$ K, and, as expected, it vanishes as $\Omega \to 0$. The gradient of the surface Green function can be calculated as (see Supplemental Material [37] for details)

$$\partial_y G_{yz} = -\partial_y G_{zy} = \frac{1}{2} \int_0^\infty dQ e^{2ik_z d} Q^3 r_p(\omega, Q), \quad (2)$$

where the integration is performed over the transverse wave vector Q, $k_z = (k^2 - Q^2)^{1/2}$ is the wave vector along z, $k = \omega/c$ is the free-space wave number, d is the particle-surface distance, and $r_p(\omega, Q)$ is the Fresnel reflection coefficient of the surface for p-polarized waves. We consider only the surface component of the Green function, because the free-space part does not contribute to the lateral force [6]. One should also notice that Eq. (2) appears in the calculation of the lateral force acting on a circularly polarized dipole oscillating at frequency ω above a surface [29]. This implies that the lateral Casimir force can be recast as the frequency integral of the dipole lateral force weighted by the appropriate frequency-dependent fluctuation terms in Eq. (1).

Numerical results.—Using Eqs. (1) and (2), we can numerically compute the lateral Casimir force for different scenarios. The material composition and size of the particle determine its isotropic nonrotating polarizability $\alpha(\omega)$ that appears in Eq. (1), while the reflection coefficient $r_p(\omega, Q)$, and therefore $\partial_y G_{yz}$, is controlled by the surface properties [see Eq. (2)]. Here we choose silicon carbide (SiC) for both the particle and the substrate. SiC is a polaritonic material that supports phonon polaritons, and its dielectric function can be modeled as $\varepsilon(\omega) = \varepsilon_\infty[1 + (\omega_L^2 - \omega_T^2)/(\omega_T^2 - \omega^2 - i\omega\gamma)]$, where $\varepsilon_\infty = 6.7$, $\hbar\omega_T = 98.3$ meV, $\hbar\omega_L = 120$ meV, and $\hbar\gamma = 0.59$ meV [38].

We gain insight into the behavior of the lateral force by examining the integrand of Eq. (1), $dF_y/d\omega$. To that end, we plot in Fig. 2(a) the imaginary part of the polarizability of SiC particles (left scale) with radius $R = 50$ nm (red curve) and $R = 500$ nm (blue curve), as obtained from the dipolar Mie coefficient [39], which therefore includes retardation that permits us to extend our results up to $kR \sim 1$. Indeed, retardation is already visible for the $R = 500$ nm particle polarizability, resulting in resonance redshift and broadening with respect to that of the $R = 50$ nm particle. Our theoretical model is based on the dipolar approximation, and therefore we expect it to be inaccurate for particle-surface distances such that the dipolar plasmon of the particle is modified by hybridization with higher-order modes. Figure 2(a) also shows the imaginary part of the reflection coefficient of a SiC surface (right scale) in the limits $Q = 0$ (gray dashed curve) and $Q \gg k$ (gray solid curve). The integrand of Eq. (1) is plotted in Fig. 2(b) for the same particles and surface as in Fig. 2(a), assuming a rotation frequency $\Omega/2\pi = 1$ kHz, temperatures $T_0 = T_1 = 300$ K, and particle-surface distances $d = 3R$

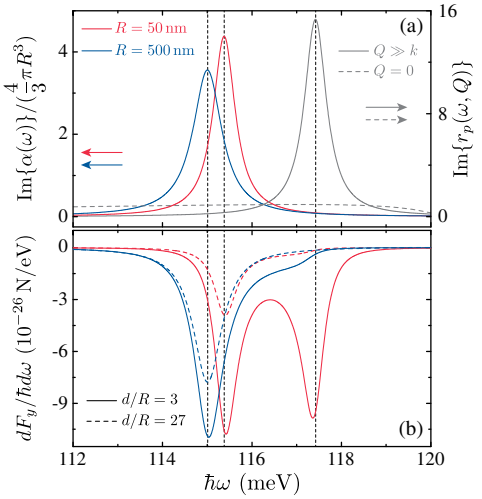

FIG. 2. (a) Imaginary part of the polarizability of SiC nanoparticles (left scale) with radius $R = 50$ nm (red curve) and $R = 500$ nm (blue curve) and imaginary part of the reflection coefficient of a SiC surface (right scale) calculated for $Q = 0$ (gray dashed curve) and for $Q \gg k$ (gray solid curve). (b) Frequency integrand of the lateral force [Eq. (1)] corresponding to the two nanoparticles of (a) when they are placed at a distance d from a SiC surface. The curves for $d/R = 27$ are multiplied by a factor of 200 to improve visibility. Moreover, we choose a rotation frequency $\Omega/2\pi = 1$ kHz and surface and particle temperatures $T_0 = T_1 = 300$ K.

(solid curves) and $d = 27R$ (dashed curves). The integrand, which can be interpreted as a force spectral density, is proportional to the difference between $\mathrm{Im}\{\alpha(\omega_+)\}N(\omega_+)$ and $\mathrm{Im}\{\alpha(\omega_-)\}N(\omega_-)$. Under realistic conditions, the rotation frequency is smaller than the particle resonance frequency ($\omega_0 \sim 100$ THz). This allows us to approximate $\mathrm{Im}\{\alpha(\omega_+)\}N(\omega_+) - \mathrm{Im}\{\alpha(\omega_-)\}N(\omega_-) \approx 2\Omega\mathrm{Im}\{\alpha(\omega)\}\partial n(T, \omega)/\partial\omega$, retaining only linear terms in Ω and assuming $T_0 = T_1 = T$. Therefore, the spectral force density, at first order in Ω, is determined by the product of $\mathrm{Im}\{\alpha(\omega)\}$ and $\mathrm{Im}\{\partial_y G_{yz}\}$, which is in turn controlled by $\mathrm{Im}\{r_p\}$. This is clearly seen in Fig. 2(b) for the $R = 50$ nm particle when $d = 3R$ (red solid curve), for which $dF_y/d\omega$ displays two peaks corresponding to $\mathrm{Im}\{\alpha\}$ and $\mathrm{Im}\{r_p\}$ in the nonretarded limit ($Q \gg k$), respectively. The second peak becomes less visible for $R = 500$ nm (blue solid curve) and completely disappears for larger separations (dashed curves) due to retardation, as expected from the nonresonant behavior of $\mathrm{Im}\{r_p\}$ when $Q = 0$.

Figure 3 shows calculations of the lateral Casimir force as a function of particle-surface separation for SiC particles of radius $R = 50$ nm (a) and $R = 500$ nm (b), rotating near a SiC surface at 1 kHz (red curves) and 100 kHz (blue curves). As expected, the lateral force shows a decreasing trend with distance. Interestingly, this trend is accompanied by an oscillatory behavior (shaded areas correspond to positive forces), which arises from the exponential term of Eq. (2), with a period of $\sim\lambda_0/2$, where $\lambda_0 = 2\pi c/\omega_0 \approx 5.4$ μm is the particle resonance wavelength. The sign oscillation of the lateral Casimir force implies that the direction and magnitude of the force can be controlled or even suppressed by choosing appropriate particle-surface separations. The dependence of the lateral Casimir force on the rotation frequency is examined in Fig. 3(c) under the same conditions as in Figs. 3(a) and 3(b). As anticipated, the value of $|F_y|$ increases linearly with Ω within the range of rotation frequencies under consideration, for which $\Omega \ll \omega_0$.

The results in Fig. 3 show that the most advantageous situation to achieve large forces involves particles rotating at high frequencies, placed close to the surface. In such cases, $dF_y/d\omega$ displays two different peaks: one associated with the polarizability of the particle and the other with the reflection coefficient of the surface [see the red solid curve in Fig. 2(b)]. Therefore, a way to enhance the force consists in bringing together these two resonances by using particles and surfaces made of different materials. This possibility is explored in Fig. 4, where the lateral Casimir force is plotted varying ω_T for the particle and the surface materials: $\omega_{T,p}$

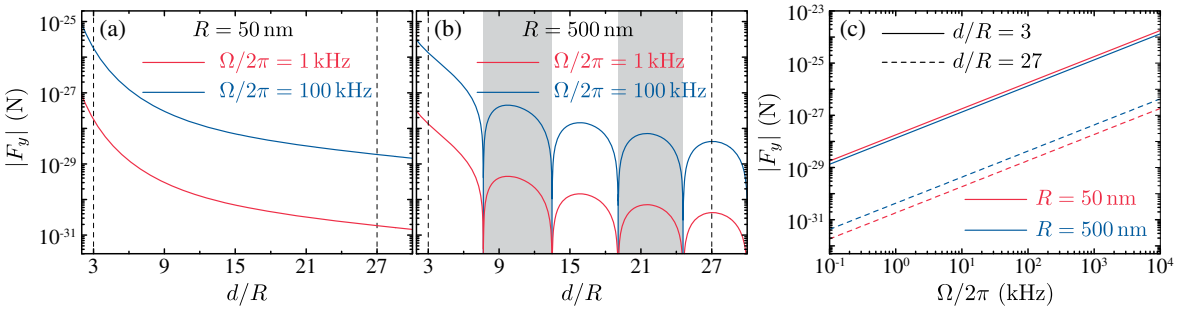

FIG. 3. (a),(b) Lateral Casimir force experienced by a SiC nanoparticle with $R = 50$ nm (a) and $R = 500$ nm (b) rotating near a SiC surface, plotted as a function of the particle-surface distance d for two different rotation frequencies: $\Omega/2\pi = 1$ kHz (red curves) and $\Omega/2\pi = 100$ kHz (blue curves). Shaded areas indicate the distances for which the lateral force is positive. (c) Lateral Casimir force for the same nanoparticles as in (a) and (b) plotted as a function of the rotation frequency Ω for particle-surface distances as indicated in the legends, which correspond to the dashed vertical lines in (a) and (b). The surface and particle temperatures are $T_0 = T_1 = 300$ K.

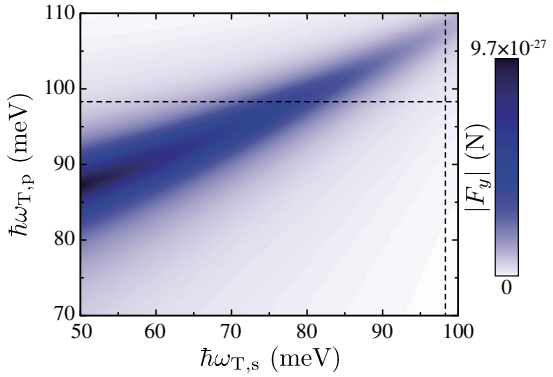

FIG. 4. Lateral force experienced by a nanoparticle of radius $R = 50$ nm plotted as a function of the transversal phonon polariton energy of the particle $\hbar\omega_{T,p}$ and the surface $\hbar\omega_{T,s}$. Other parameters of the particle and surface dielectric function are taken as those of SiC (see main text), the particle-surface distance is $d = 3R$, the rotation frequency is $\Omega/2\pi = 1$ kHz, and the temperatures are $T_0 = T_1 = 300$ K. The dashed lines correspond to $\hbar\omega_T = 98.3$ eV as in SiC.

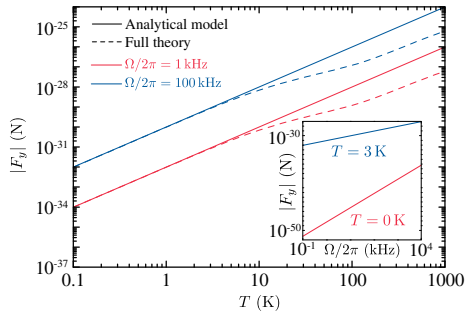

FIG. 5. Lateral force experienced by a graphite nanoparticle of radius $R = 10$ nm plotted as a function of the particle and surface temperatures, which are taken to be equal ($T_0 = T_1 = T$), for two different rotation frequencies. Dashed curves correspond to calculations using the full theory, while solid curves indicate the results obtained with the analytical model described in the text. The inset shows the lateral force as a function of rotation frequency for two different temperatures calculated using the analytical model. In all cases, the particle-surface distance is $d = 3R$.

and $\omega_{T,s}$, respectively. For simplicity, we keep the values of ε, ω_L, and γ the same as in SiC. Examining Fig. 4, we observe that the lateral Casimir force can be greatly enhanced with respect to a homogeneous SiC system (corresponding to the crossing of the dashed lines) when $\omega_{T,p} > \omega_{T,s}$ and the particle and surface resonances overlap.

Analytical limit for metallic media.—It is possible to obtain a closed-form analytical expression of the lateral Casimir force for the case of metallic materials, whose response at low frequencies, well below interband transitions, can be described in terms of the static conductivity σ_0 using a Drude dielectric function $\varepsilon(\omega) = 1 + 4\pi i\sigma_0/\omega$. When the relevant frequencies Ω and $k_B T/\hbar$ are much smaller than σ_0, we can approximate $\mathrm{Im}\{\alpha\} \approx (3\omega R^3)/(4\pi\sigma_0)$, $\mathrm{Im}\{r_p\} \approx \omega/(2\pi\sigma_0)$, and $\mathrm{Im}\{\partial_y G_{yz}\} \approx (3\omega)/(32\pi d^4\sigma_0)$. Using these expressions in Eq. (1), we obtain the following result for the lateral force:

$$F_y = -\frac{3\hbar}{256\pi^3\sigma_0^2}\frac{R^3}{d^4}\left(\frac{4\pi^2 k_B^2}{\hbar^2}(T_1^2 + T_0^2) + 2\Omega^2\right)\Omega. \quad (3)$$

Interestingly, multiplying F_y by d we obtain the expression of the torque acting on the particle that was derived in Ref. [21], exactly as one would expect for a wheel of radius d based on classical-mechanics arguments, which is consistent with the conservation of angular momentum in the combined particle-surface system. This hence reinforces our interpretation of the studied system as the Casimir analogue of a mechanical wheel rotating and moving on a surface but without the necessity of contact between them.

Figure 5 shows the lateral force for a $R = 10$ nm particle made of graphite, for which $\sigma_0 = 2.1 \times 10^{14}$ s^{-1}, rotating at a distance $d = 3R$ from a surface of the same material, plotted as a function of the temperature T (we take $T_1 = T_0 = T$). Solid curves correspond to the results of the analytical model, while dashed ones show the calculations obtained with the full theory using a tabulated dielectric function [40]. As expected, the analytical model agrees well with the full theory for low temperatures ($T \lesssim 10$ K), for which the lateral force shows a quadratic dependence on temperature, as expected from Eq. (3). Incidentally, Eq. (3) also predicts a cubic dependence of the lateral force on the rotation frequency at zero temperature (i.e., $F_y \propto \Omega^3$ for $T_1 = T_0 = 0$ K), which is in sharp contrast with the linear behavior obtained for finite temperatures, as shown in the inset to Fig. 5.

Concluding remarks.—In summary, we have predicted the existence of a lateral Casimir force acting on rotating particles near planar surfaces. This force arises from the symmetry breaking induced by the particle rotation on the left- and right-handed components of the vacuum and thermal fluctuations of the electromagnetic field; therefore, it is intimately related to the recently discovered lateral optical force acting on circularly polarized dipoles placed near a surface. The sign and magnitude of the lateral Casimir force depends on the geometrical and material properties of the particle and the surface, allowing tunability of the force direction and magnitude and even complete suppression at certain particle-surface separations. A possible experimental verification could involve the use of fullerenes, which present strong vibrational resonances in the infrared and, due to their small moment of inertia and strong robustness, can rotate with very large frequencies in the order of 100 GHz [41]. The lateral force would be detected by measuring the deflection in the trajectory of a hypothermal beam of fullerenes directed toward a surface. The action of the lateral force, in contrast to that of the conventional

Casimir force, will be cumulative along the incident and reflected trajectory, thus resulting in a measurable effect. The presented results describe a new type of lateral Casimir force acting on nanostructures, which is important for understanding, engineering, and controlling dynamic dispersion interactions at the nanoscale.

A. M. acknowledges financial support from the Department of Physics and Astronomy and the College of Arts and Sciences of the University of New Mexico, and the University of New Mexico (UNM) Center for Advanced Research Computing for computational resources used in this work. F. J. G. de A. acknowledges support from the Spanish MINECO (MAT2014-59096-P and SEV2015-0522), Fundació privada CELLEX, and Agència de Gestió d'Ajuts Universitaris i de Recerca (AGAUR) (2014-SGR-1400). F. J. R.-F. was supported by the European Research Council Project No. ERC-2016-STG-714151-PSINFONI. A. V. Z. acknowledges support from the Engineering and Physical Sciences Research Council (United Kingdom), the European Research Council project iPLASMM (321268), the Royal Society and the Wolfson Foundation.

*manjavacas@unm.edu
†francisco.rodriguez_fortuno@kcl.ac.uk

[1] H. B. G. Casimir, Proc. K. Ned. Akad. Wet. **51**, 793 (1948).
[2] S. Lamoreaux, Phys. Today **60**, 2, 40 (2007).
[3] D. Dalvit, P. Milonni, D. Roberts, and F. da Rosa, *Casimir Physics*, Lect. Notes Phys. (Springer, Berlin, 2011).
[4] J. N. Munday and F. Capasso, Int. J. Mod. Phys. A **25**, 2252 (2010).
[5] P. Ball, Nature (London) **447**, 772 (2007).
[6] A. W. Rodriguez, F. Capasso, and S. G. Johnson, Nat. Photonics **5**, 211 (2011).
[7] C. Henkel, K. Joulain, J. P. Mulet, and J. J. Greffet, J. Opt. A **4**, S109 (2002).
[8] A. O. Sushkov, W. J. Kim, D. A. R. Dalvit, and S. K. Lamoreaux, Nat. Phys. **7**, 230 (2011).
[9] R. Golestanian and M. Kardar, Phys. Rev. Lett. **78**, 3421 (1997).
[10] T. Emig, A. Hanke, R. Golestanian, and M. Kardar, Phys. Rev. Lett. **87**, 260402 (2001).
[11] F. Chen, U. Mohideen, G. L. Klimchitskaya, and V. M. Mostepanenko, Phys. Rev. Lett. **88**, 101801 (2002).
[12] D. A. R. Dalvit, P. A. M. Neto, A. Lambrecht, and S. Reynaud, J. Phys. A **41**, 164028 (2008).
[13] T. Emig, A. Hanke, R. Golestanian, and M. Kardar, Phys. Rev. A **67**, 022114 (2003).
[14] E. V. Blagov, G. L. Klimchitskaya, U. Mohideen, and V. M. Mostepanenko, Phys. Rev. A **69**, 044103 (2004).
[15] A. Ashourvan, M. F. Miri, and R. Golestanian, Phys. Rev. Lett. **98**, 140801 (2007).
[16] H.-C. Chiu, G. L. Klimchitskaya, V. N. Marachevsky, V. M. Mostepanenko, and U. Mohideen, Phys. Rev. B **81**, 115417 (2010).
[17] M. Nasiri, A. Moradian, and M. F. Miri, Phys. Rev. E **82**, 037101 (2010).
[18] B. Müller and M. Krüger, Phys. Rev. A **93**, 032511 (2016).
[19] A. Manjavacas and F. J. García de Abajo, Phys. Rev. Lett. **105**, 113601 (2010).
[20] A. Manjavacas and F. J. García de Abajo, Phys. Rev. A **82**, 063827 (2010).
[21] R. Zhao, A. Manjavacas, F. J. García de Abajo, and J. B. Pendry, Phys. Rev. Lett. **109**, 123604 (2012).
[22] J. B. Pendry, J. Phys. Condens. Matter **9**, 10301 (1997).
[23] K. Y. Bliokh and F. Nori, Phys. Rev. A **85**, 061801 (2012).
[24] K. Y. Bliokh, A. Y. Bekshaev, and F. Nori, Nat. Commun. **5**, 3300 (2014).
[25] A. Aiello, P. Banzer, M. Neugebauer, and G. Leuchs, Nat. Photonics **9**, 789 (2015).
[26] K. Y. Bliokh, F. J. Rodríguez-Fortuño, F. Nori, and A. V. Zayats, Nat. Photonics **9**, 796 (2015).
[27] S. Scheel, S. Y. Buhmann, C. Clausen, and P. Schneeweiss, Phys. Rev. A **92**, 043819 (2015).
[28] S. Sukhov, V. Kajorndejnukul, R. R. Naraghi, and A. Dogariu, Nat. Photonics **9**, 809 (2015).
[29] F. J. Rodríguez-Fortuño, N. Engheta, A. Martínez, and A. V. Zayats, Nat. Commun. **6**, 8799 (2015).
[30] F. J. Rodríguez-Fortuño, G. Marino, P. Ginzburg, D. O'Connor, A. Martínez, G. A. Wurtz, and A. V. Zayats, Science **340**, 328 (2013).
[31] J. P. B. Mueller and F. Capasso, Phys. Rev. B **88**, 121410 (2013).
[32] F. Le Kien and A. Rauschenbeutel, Phys. Rev. A **90**, 023805 (2014).
[33] H. Nyquist, Phys. Rev. **32**, 110 (1928).
[34] H. B. Callen and T. A. Welton, Phys. Rev. **83**, 34 (1951).
[35] L. Novotny and B. Hecht, *Principles of Nano-Optics* (Cambridge University Press, Cambridge, England, 2006).
[36] J. P. Gordon and A. Ashkin, Phys. Rev. A **21**, 1606 (1980).
[37] See Supplemental Material at http://link.aps.org/supplemental/10.1103/PhysRevLett.118.133605 for more details on the theory and the derivation of Eqs. (1) and (2).
[38] E. D. Palik, *Handbook of Optical Constants of Solids* (Academic, San Diego, 1985).
[39] V. Myroshnychenko, J. Rodríguez-Fernández, I. Pastoriza-Santos, A. M. Funston, C. Novo, P. Mulvaney, L. M. Liz-Marzán, and F. J. García de Abajo, Chem. Soc. Rev. **37**, 1792 (2008).
[40] B. T. Draine, Astrophys. J. **598**, 1026 (2003).
[41] M. Dresselhaus, G. Dresselhaus, and P. Eklund, *Science of Fullerenes and Carbon Nanotubes* (Academic, San Diego, 1996).